

AKÜ FEMÜBİD 23 (2023) 015901 (228-246)

AKU J. Sci. Eng. 23 (2023) 015901 (228-246)

DOI: 10.35414/akufemubid.1071280

Araştırma Makalesi / Research Article

Dynamic and Buckling Analysis of the Laminated Composite Curved Plate Frame Structures

Oguzhan DAS^{1,2*}, Hasan OZTURK³, Can GONENLI⁴¹ National Defence University, Air NCO Vocational School, Department of Aeronautics Sciences, Izmir, Türkiye.² Dokuz Eylül University, The Graduate School of Natural and Applied Sciences, Izmir, Türkiye.³ Dokuz Eylül University, Department of Mechanical Engineering, Izmir, Türkiye.⁴ Ege University, Ege Vocational School, Department of Machine Construction and Drawing, Izmir, Türkiye.*Corresponding Author e-mail^{1,2}: odas@msu.edu.tre-mail³: hasan.ozturk@deu.edu.tre-mail⁴: can.gonenli@ege.edu.trORCID: <https://orcid.org/0000-0001-7623-9278>ORCID: <https://orcid.org/0000-0002-8308-8428>ORCID: <https://orcid.org/0000-0001-9163-1569>

Geliş Tarihi: 10.02.2022

Kabul Tarihi: 12.01.2023

Abstract

Keywords

Dynamic Stability;
Vibration; Buckling;
Composite Structures;
Finite Element
Analysis; Curved Plate
Frames

This study presents the dynamic and buckling analysis of the laminated composite thin arch plate frame structures employing Classical Plate Theory with Finite Element Analysis. For this purpose, the effects of the radius of curvature, aspect ratio, and stacking order of such structures on the first ten natural frequencies, mode shapes, critical buckling load, and the first unstable regions are investigated. Besides, the two-bay curved plate frame structure is investigated. In order to perform dynamic and buckling analyses, a computer code is developed and executed via MATLAB. The results are compared and validated with those of ANSYS. It is concluded that the aspect ratio or the stacking order affects the dynamic characteristics of the curved plate frame structure considerably while the radius of curvature relatively has less impact on such dynamic properties of the structure.

Elyaflı Kompozit Eğri Plaka Çerçevelerin Dinamik ve Burkulma Analizi

Öz

Anahtar kelimeler

Dinamik Kararlılık;
Titreşim; Burkulma;
Kompozit Yapılar;
Sonlu Elemanlar
Analizi; Eğri Plaka
Çerçeveler

Bu çalışma, ince eğri elyafli kompozit plaka çerçeve yapıların dinamik ve burkulma analizlerini Klasik Plaka Teorisi ve Sonlu Elemanlar Analizi ile incelemektedir. Bu amaçla, yapının eğrilik yarıçapının, en-boy oranının ve elyaf düzeninin ilk on doğal frekans, mod şekilleri, kritik burkulma yükü ve birinci dinamik kararlılık bölgeleri üzerine olan etkileri araştırılmıştır. Ayrıca, iki bölümlü yapı da ele alınmıştır. Dinamik ve burkulma analizleri MATLAB üzerinden bir bilgisayar kodu aracılığı ile gerçekleştirilmiştir. Buradan elde edilen sonuçlar aynı analizlerin ANSYS üzerinden gerçekleştirilmesi ile doğrulanmıştır. Sonuçlar olarak yapının en-boy oranının ve laminasyon düzeninin dinamik özellikleri büyük ölçüde etkilediği, eğrilik yarıçapının ise diğer parametrelere göre yapının dinamik özellikleri üzerinde daha az etki oluşturduğu görülmüştür.

© Afyon Kocatepe Üniversitesi

1. Introduction

Curved structures are widely used in the aerospace industry due to their effectiveness and existence in aero-frames. Additionally, composite materials are extensively considered in the aerospace industry to improve structural efficiency and lower the weight of the aero-structure. Evaluating the dynamic and buckling characteristics of such structures is

essential since vibration and critical loading conditions

may result in damage or complete failure. Researchers have been interested in investigating the dynamic and buckling properties of various structures for many years. Since it is impossible to mention all of these works, some studies of those are presented as follows. Marjanovic *et al.* (2017) used a dynamic

stiffness element based on the first-order shear deformation theory and higher-order shear deformation theory to perform free vibration analysis of composite plates. They investigated the effects of the boundary conditions and plate side on the thickness and orthotropy ratios on the low and high modes of vibration. Serdoun and Cherif (2016) investigated the free vibration analysis of composite thick rectangular plates using higher-order shear deformation theory. (Chen *et al.* 2017) presented the free vibration analysis of composite truss core sandwich plates using third-order shear deformation theory and zig-zag theory. (Demir *et al.* 2017) investigated free vibration analysis of annular sector plates using conical shell equations, first-order shear deformation theory, discrete singular convolution, and differential quadrature. (Shankar and Mahato 2017) presented the vibration analysis of composite plates having delamination and/or damages using the finite element method. (Tornabene *et al.* 2018) investigated free vibration analysis of laminated plates and shells, considering two different approaches, differential quadrature, and integral quadrature. (Abulanour *et al.* 2018) studied the free vibration analysis of simply supported functionally graded plates using a new shear deformation theory that comprises the stretching effect. (Vidal *et al.* 2019) investigated the free vibration analysis of laminated composite plates by using a variable separation approach. (Thakur *et al.* 2020) employed an efficient C0 finite element modeling combined with higher-order non-polynomial shear deformation theory to investigate the natural frequencies and to perform a transient analysis of the laminated composite folded plates having different fiber angles, fold location, crack angle, lamination scheme, and boundary conditions. (Rezaiee-Pajand *et al.* 2020) performed free vibration analysis of functionally graded hybrid matrix/fiber nanocomposite conical shells employing the First-Order Shear Deformation Theory. They solved the Donell-type governing differential equations by using the Generalized Differential Quadrature Method. They investigated the effects of the boundary condition, material, and geometric properties on the dimensionless frequency of the nanocomposite conical shell. (Fang

et al. 2020) examined the vibration and thermal buckling characteristics of rotating nonlocal functionally graded nanobeams by using Eringen's nonlocal elasticity theory (ENET) and Euler Bernoulli Beam Theory. They investigated the effects of the hub radius ratio, temperature difference, material gradient index, slenderness ratio, dimensionless angular velocity, and nonlocal parameters on the natural frequencies and critical temperatures that cause buckling of the rotating functionally graded nanobeams.

When a structure is subjected to a static load, it may face a critical phenomenon called buckling. There are lots of studies that dealt with the buckling of structures such as beams, plates, or frames. Some of those are mentioned as follows. (Bourada *et al.* 2016) studied buckling analysis of isotropic and ortho-tropic plates by introducing a novel four-variable refined plate theory. (Hao *et al.* 2017) investigated the buckling analysis of composite variable stiffness panels considering the Mindlin plate theory. (Chikh *et al.* 2017) presented a thermal buckling analysis of cross-ply laminated composite plates using a simplified higher-order shear deformation theory. (Zghal *et al.* 2018) studied the buckling behavior of functionally graded materials and nano-tubes reinforced composite flat and curved plates using a double-directors finite element shell model.

If a structure is subjected to dynamic loads, it is parametrically exciting. Therefore, dynamic instability may occur even if damping exists. This phenomenon occurs because of the amplitudes of the response that increase exponentially. Hence researchers addressed many studies about the dynamic stability of structures due to their significance. Some of these studies are presented as follows. (Fazilati 2017) performed the stability analysis of variable stiffness laminated composite plates that have delaminations by using the finite strip method. (Samukham *et al.* 2018) investigated dynamic stability analysis of variable angle tow composite with delamination placed around a cut-out under simply supported boundary conditions. They used the first-order shear deformation theory and finite element method to evaluate the governing equations of variable angle tow

composite structure. (Shafei *et al.* 2019) investigated the dynamic stability analysis of anisotropic composite materials using the iso-geometric analysis based on higher-order shear deformation theory.

In this study, dynamic analysis of laminated composite curved thin plate frames is investigated. Although there are many studies concerning the dynamic analysis of structures, to the best of the Authors' knowledge, there are no reported works that cover the dynamic properties of laminated composite curved frame structures in the literature. The effects of the radius of curvature, aspect ratio, and fiber orientation on the first ten natural frequencies and corresponding mode shapes, critical buckling loads, and the first unstable regions are investigated. For these purposes, the Classical Plate Theory is employed with the Finite Element Method.

2. Mathematical Expressions

Finite element analysis is performed to perform free vibration, buckling, and dynamic stability analyses of curved plate frames, shown in Fig. 1. Four node quadrilateral element shown in Fig. 2, is utilized to model the curved plate frame structures. Considering the Classical Plate Theory, Each node has five degrees of freedom (DOF), $u, v, w, \theta_x,$ and θ_y . Eq. (1) gives general displacement functions of a finite element as a summation of the nodal displacements (Petyt 2015).

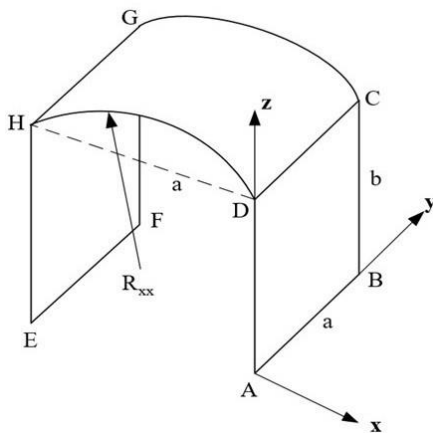


Figure 1. A curved plate frame structure

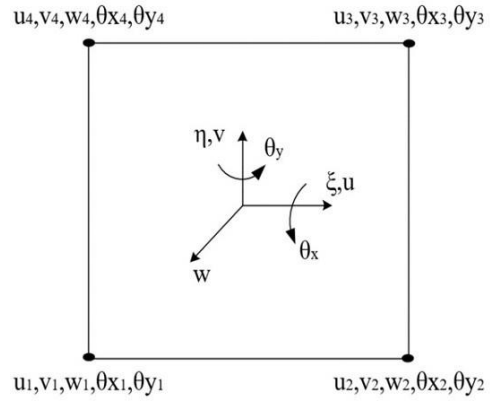


Figure 2. Four node quadrilateral element.

$$\begin{aligned} \{u\} &= \sum_{i=1}^4 N_{m_i} \{u_i\} \\ \{v\} &= \sum_{i=1}^4 N_{m_i} \{v_i\} \\ \begin{Bmatrix} w \\ \theta_x \\ \theta_y \end{Bmatrix} &= \sum_{i=1}^4 N_{b_i} \begin{Bmatrix} w_i \\ \theta_{x_i} \\ \theta_{y_i} \end{Bmatrix}, i = 1, \dots, 4 \end{aligned} \tag{1}$$

$$u(x, y, z) = u_0(x, y) - z\theta_y, \quad \theta_y = \frac{\partial w_0}{\partial x}$$

$$v(x, y, z) = v_0(x, y) - z\theta_x, \quad \theta_x = \frac{\partial w_0}{\partial y}$$

$$w(x, y, z) = w_0(x, y)$$

where N_m and N_b are the shape functions (Petyt 2015) for in-plane and out-of-plane displacements, respectively.

$$\begin{aligned} N_{m_i} &= \frac{1}{4} [(1 + \xi_j \xi)(1 + \eta_j \eta)] \\ N_{b_i} &= \frac{1}{8} \begin{bmatrix} (1 + \xi_i \xi)(1 + \eta_j \eta)(2 + \xi_i \xi + \eta_j \eta - \xi^2 - \eta^2) \\ b(1 + \xi_i \xi)(\eta_j + \eta)(\eta^2 - 1) \\ -a(\xi_j + \xi)(\xi^2 - 1)(1 + \eta_j \eta) \end{bmatrix} \end{aligned} \tag{2}$$

$$i, j = 1, \dots, 4$$

where $a, b, \epsilon,$ and η are the length, width, and natural coordinates of the four-node quadrilateral element. Eq.(3) gives the strain energy of the finite element U_e (Petyt 2015).

$$U_e = \frac{1}{2} \int_V \{\sigma\}_k^T \{\epsilon\} dV \tag{3}$$

where $\{\sigma\}^T$ denotes the stress components matrix of the k^{th} layer and $\{\epsilon\}$ is the strain matrix.

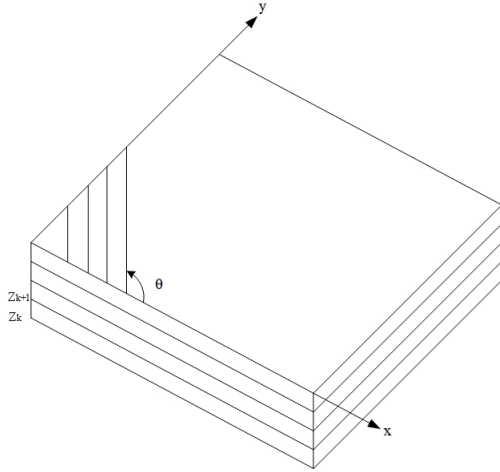


Figure 3. Laminated composite material

For a laminated composite structure, shown in Fig. 3, the constitutive relation between the stress tensor matrix and the material modulus matrix $[Q]_k$ is given as

$$\{\sigma\}_k^T = [Q]_k \{\epsilon\} \quad (4)$$

or

$$\begin{bmatrix} \sigma_{xx} \\ \sigma_{yy} \\ \tau_{xy} \end{bmatrix}^k = \begin{bmatrix} Q_{11} & Q_{12} & Q_{16} \\ Q_{12} & Q_{22} & Q_{26} \\ Q_{16} & Q_{26} & Q_{66} \end{bmatrix}^k \begin{bmatrix} \epsilon_{xx} \\ \epsilon_{yy} \\ \gamma_{xy} \end{bmatrix}^k \quad (5)$$

where

$$\begin{aligned} Q_{11} &= q_{11}c^4 + 2(q_{11} + 2q_{66})s^2c^2 + q_{22}s^4 \\ Q_{12} &= (q_{11} + q_{22} - 4q_{66})s^2c^2 + q_{12}(s^4 + c^4) \\ Q_{22} &= q_{11}s^4 + 2(q_{11} + 2q_{66})s^2c^2 + q_{22}c^4 \\ Q_{16} &= (q_{11} - q_{12} - 2q_{66})sc^3 \\ &\quad + (q_{12} - q_{22} + 2q_{66})s^3c \\ Q_{26} &= (q_{11} - q_{12} - 2q_{66})s^3c \\ &\quad + (q_{12} - q_{22} + 2q_{66})sc^3 \\ Q_{66} &= (q_{11} + q_{12} - 2q_{12} - 2q_{66})s^2c^2 + q_{66}(s^4 \\ &\quad + c^4) \end{aligned} \quad (6)$$

where c and s are $\cos\theta$ and $\sin\theta$ in which θ stands for the fiber angle. The material stiffness components q_{ij} ($i, j=1, 2, 6$) are calculated as

$$\begin{aligned} q_{11} &= \frac{E_x}{1 - \nu_{xy}\nu_{yx}} \\ q_{12} &= \frac{\nu_{xy}E_x}{1 - \nu_{xy}\nu_{yx}} \\ q_{22} &= \frac{E_y}{1 - \nu_{xy}\nu_{yx}} \\ q_{66} &= G_{xy} \end{aligned} \quad (7)$$

where E_x and E_y are the modulus of elasticity in x - and y - direction. G_{xy} is the shear modulus with respect to x -, y - direction. ν_{xy} and ν_{yx} represent the strain in x - and y - direction due to the unit strain in y - and x - direction, respectively (Petyt 2015) Substituting Eqs. (1) and (4) into Eq.(3) gives

$$U_e = \frac{1}{2} \int_A \{\epsilon\}^T \mathbf{D}_m \{\epsilon\} dA \quad (8)$$

where $\{\epsilon\}$ denotes the strain components as,

$$\{\epsilon\} = \begin{Bmatrix} \frac{\delta u}{\delta \epsilon} \\ \frac{\delta v}{\delta \eta} \\ \frac{\delta u}{\delta \eta} + \frac{\delta v}{\delta \epsilon} \\ \frac{\delta^2 w}{\delta \epsilon^2} \\ \frac{\delta^2 w}{\delta \eta^2} \\ \frac{\delta^2 w}{\delta \eta \delta \epsilon} \end{Bmatrix} \quad (9)$$

and \mathbf{D}_m is the material stiffness matrix given as,

$$\mathbf{D}_m = \begin{bmatrix} \mathbf{A} & \mathbf{B} \\ \mathbf{B} & \mathbf{C} \end{bmatrix} \quad (10)$$

where \mathbf{A} , \mathbf{B} , and \mathbf{C} are the longitudinal, bending-longitudinal coupled, and bending stiffness matrices, which are

$$\begin{aligned} \mathbf{A} &= \sum_{k=1}^{NL} [Q]_k (z_k - z_{k-1}) \\ \mathbf{B} &= \frac{1}{2} \sum_{k=1}^{NL} [Q]_k (z_k^2 - z_{k-1}^2) \end{aligned} \quad (11)$$

$$C = \frac{1}{3} \sum_{k=1}^{NL} [Q]_k (z_k^3 - z_{k-1}^3)$$

where NL is the number of layer and z_k is the thickness of the k^{th} layer. The strain energy can be written in matrix form as

$$U_e = \{q_e\}^T \mathbf{k}_e \{q_e\} \tag{12}$$

where $\{q_e\}$ is,

$$\{q_e\} = \sum_{i=1}^4 [u_i \ v_i \ w_i \ \theta_{x_i} \ \theta_{y_i}] \tag{13}$$

and \mathbf{k}_e is the element stiffness matrix (Petyt 2015). The kinetic energy of the finite element is

$$T_e = \frac{1}{2} \rho h \int_A (\dot{u}^2 + \dot{v}^2 + \dot{w}^2) dA \tag{14}$$

where ρ is the density of the material and h denotes the thickness of the finite element. The kinetic energy equation can be written in matrix form as

$$T_e = \{q_e\}^T \mathbf{m}_e \{q_e\} \tag{15}$$

where \mathbf{m}_e is the element mass matrix (Petyt 2015).

If a structure is subjected to a load as shown in Fig. 4(a), the phenomenon called buckling may occur. In this study, the distributed loading condition is assumed as a point loading condition as shown in Fig. 4(b) The work done by that load can be evaluated as

$$V_e = \frac{1}{2} \int_A \left(P_x \left(\frac{\partial w}{\partial x} \right)^2 + 2P_{xy} \frac{\partial w}{\partial x} \frac{\partial w}{\partial y} + P_y \left(\frac{\partial w}{\partial y} \right)^2 \right) dA \tag{16}$$

where P_x , P_{xy} , and P_y represent the applied compressive and shear loads regarding the x- and y-axis of the transformed coordinate system of ABCD and EFGH plates.

Since the equivalent point load is applied along the x-direction of the transformed coordinate system of the ABCD and EFGH plates, only P_x is taken into account. Therefore Eq.(16) becomes

$$V_e = \frac{1}{2} \int_A P_x \left(\frac{\partial w}{\partial x} \right)^2 dA \tag{17}$$

Eq. (17) can be written regarding Eq.(2) as

$$V_e = \frac{1}{2} \int \int \{q_e\}^T [B_G]^T P_x [B_G] \{q_e\} d\xi d\eta \tag{18}$$

where

$$B_G = \begin{bmatrix} 0 & 0 & 0_{1 \times 3} \\ 0 & 0 & 0_{1 \times 3} \\ 0_{3 \times 1} & 0_{3 \times 1} & \frac{\partial N_b}{\partial x} \quad 0_{3 \times 3} \end{bmatrix} \tag{19}$$

The work done by the point load can be written in matrix form as (Dey and Singha 2006)

$$V_e = \{q_e\}^T \mathbf{k}_{ge} \{q_e\} \tag{20}$$

Substituting Eq.(19) into Eq.(17) gives \mathbf{k}_{ge} as

$$\mathbf{k}_{ge} = [B_G]^T P_x [B_G] \tag{21}$$

where P_x is the equivalent point load, which is assumed as

$$P_x = Wab \tag{22}$$

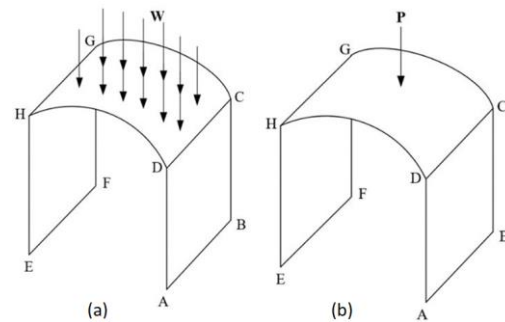


Figure 4. (a)The distributed loading condition and (b) the equivalent point loading condition of single-bay laminated composite curved plate frame structure.

Both the curvature and the frame geometry of the structure, shown in Fig. 1, are modeled by flat finite elements shown in Fig. 2. Hence the local coordinates of each element matrix should be transformed when necessary to satisfy all degrees of freedom (DOF) of the structure. Hence, to obtain the curvature and frame geometry, each element matrix is transformed as

$$\begin{aligned}
 k_{et} &= T^T k_e T \\
 m_{et} &= T^T m_e T \\
 k_{get} &= T^T k_{ge} T
 \end{aligned}
 \tag{23}$$

where k_{et} , m_{et} , and k_{get} are the transformed element stiffness, mass, and geometry matrices, respectively. T is the transformation matrix, which is given as

$$T = \begin{bmatrix} \cos\beta & 0 & \sin\beta & 0 & 0 & 0 \\ 0 & 1 & 0 & 0 & 0 & 0 \\ -\sin\beta & 0 & \cos\beta & 0 & 0 & 0 \\ 0 & 0 & 0 & \cos\beta & 0 & \sin\beta \\ 0 & 0 & 0 & 0 & 1 & 0 \\ 0 & 0 & 0 & -\sin\beta & 0 & \cos\beta \end{bmatrix}
 \tag{24}$$

where β is the rotation angle around y-axis, as shown in Fig.5.

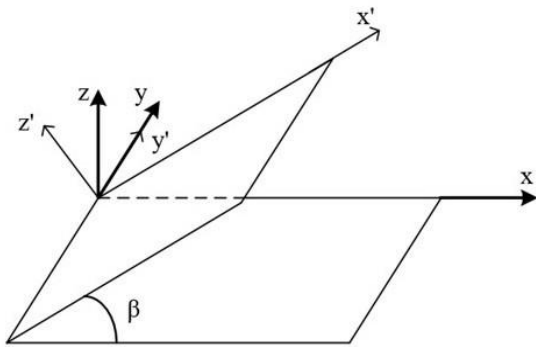


Figure 5. Transformation of local coordinates.

It is seen from Eq.(20) that the transformation matrix requires 6-DOF while there are 5-DOF according to the displacement functions given in Eq.(1). Therefore the drilling effect (θ_z) has to be considered. However, according to the displacement functions of the Classical Plate Theory, given in Eq.(1), it is seen that the drilling effect is neglected. Hence, θ_z is added for each node to obtain a suitable 6-DOF finite element. During the addition process, it is considered that the corresponding non-diagonal terms are set to zero whereas the diagonal terms of θ_z are set to be 1000 times smaller than the minimum value of the corresponding element matrix.

Structural dynamic loadings may cause dynamic instability by means of parametric resonance.

Hence, it is significant to find the unstable and stable regions of structures. Dynamic instability problem can be solved as an eigenvalue problem. The equivalent loading case shown in Fig. 4(b), can be considered as a periodic load, $P(t)$. Such a periodic load can be formulated in terms of the periodic axial compressive load as $P(t) = P + P_t \cos\lambda t$, where λ is the excitation frequency, P and P_t denote the static and time-dependent periodic compressive load, respectively. The static and time-dependent periodic compressive load components can be written by means of the fraction of the static critical buckling load, (P_{cr}) as

$$\begin{aligned}
 P(t) &= \alpha P_{cr} + \beta P_{cr} \cos\lambda t \\
 \alpha &= \frac{P}{P_{cr}} \\
 \beta &= \frac{P_t}{P_{cr}}
 \end{aligned}
 \tag{25}$$

where α is the static load factor and β is the dynamic load factor. The dynamic response of the structure can be written in terms of Lagrange's equation of motion in matrix form as

$$M\ddot{q} + Kq - P(t)K_g q = 0
 \tag{26}$$

Substituting Eq.(25) into Eq.(26) gives the equation of motion as (Bolotin, 1964)

$$M\ddot{q} + (K - P_{cr}(\alpha + \beta \cos\lambda t)K_g)q = 0
 \tag{27}$$

Performing a periodic solution considering the period as $2T = \pi/\lambda$ provides practical significance since the width of the first unstable regions is generally larger than those of the period T , according to Bolotin (1964). Therefore, the eigenvalue problem of the dynamic stability analysis considering $2T$ period can be written as

$$\left[K - P_{cr}(\alpha \pm 0.5\beta)K_g - \frac{\lambda^2}{4}M \right] q = 0
 \tag{28}$$

The eigenvalue problem of dynamic stability analysis given in Eq.(28) can be formed into:

- (i) An eigenvalue problem of free vibration analysis if $\alpha = \beta = 0$ and $\omega = \lambda/2$, where ω is the natural frequency of the structure.

- (ii) An eigenvalue buckling problem or a static stability problem if $\alpha = 1$, $\beta = 0$, and $\lambda = 0$.
- (iii) An eigenvalue dynamic stability problem if all terms exist.

3. Numerical Results

This study presents the dynamic and buckling analysis of the laminated composite arch plate frame structures, shown in Fig. 1. The geometric and material properties of such structures are given in Table 1. The effects of the stacking order, the radius of curvature (R_{xx}), and aspect ratio (a/b) on the first ten natural frequency values, critical buckling loads, and the first unstable regions of the structure are investigated. Besides, the two-bay curved plate frame structure is examined. The analyses are performed under fixed from all ends boundary conditions. For simplicity, the stacking orders including the fiber angle of each layer are denoted as follows.

$$C1 = [(0^0)]_4, C2 = [(90^0/0^0)]_{2s}, C3 = [(0^0/90^0)]_{2s}$$

$$C4 = [0^0/45^0/-45^0/0^0], C5 = [0^0/60^0/-60^0/0^0]$$

The accuracy of the results is validated by performing a convergence analysis considering ANSYS results. Fig. 6 shows the convergence analysis results considering the 15x15, 20x20, 25x25, and 30x30 elements for the entire arch plate frame structure. It is seen that the structure was represented accurately for 30x30 elements. However, the accuracy changes for the sixth and seventh modes. It is concluded that the representation of the considered finite element may reduce for bending and torsional modes in which the maximum displacement occurs at the curved section of the structure (see Appendix A). However, such a reduction is not significant and increasing the element number may diminish the error rate. Tables 1 and 2 give the material properties and the convergence analysis results of the buckling analysis for laminated composite arch plate frame structure having C1 stacking order and $R_{xx} = 2a$ radius of curvature. Similar to the natural frequency results, the best accuracy is obtained for 30x30 elements. Hence, all analyses are performed by using 30x30 number of elements.

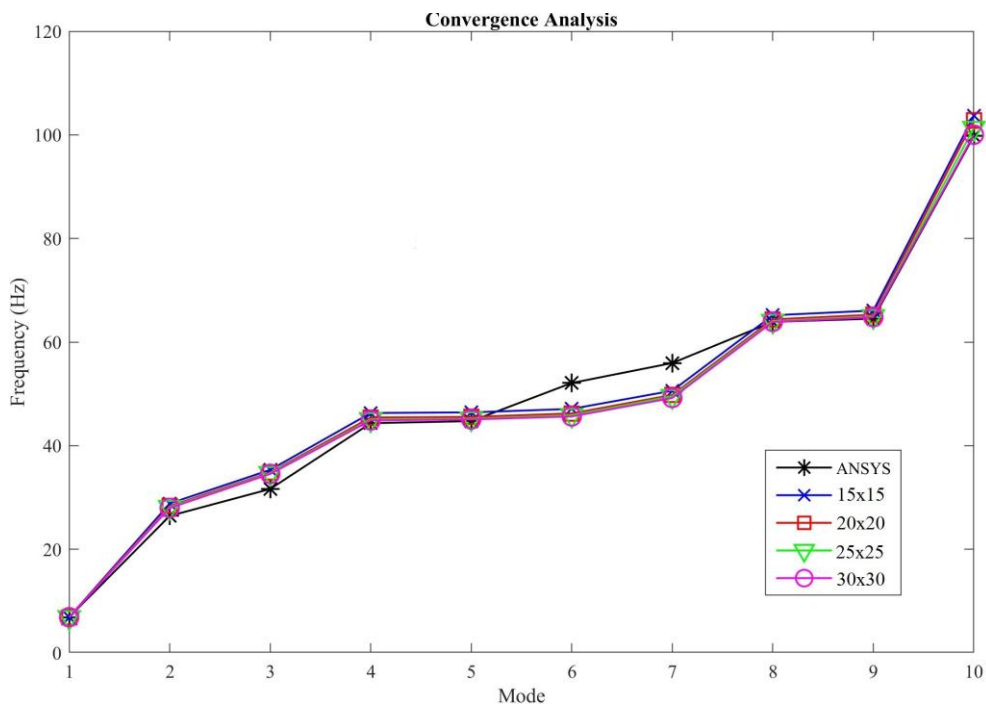


Figure 6. Free vibration convergence analysis results.

Table 1. Material and geometry properties of the laminated composite curved frame structures.

Property	Symbol	Quantity
Longitudinal Elasticity Modulus	E_x	45 GPa
Transverse Elasticity Modulus	E_y	12 GPa
Shear Modulus	G_{xy}	7.2 GPa
Density	ρ	2080 kg/m ³
Poisson Ratio	ν	0.33
Geometric Properties of the Structure		
Plate component length and width	a,b	1000 mm
Thickness	h	10 mm
Radius of Curvature	R_{xx}	2a

Table 2. Buckling convergence analysis results.

Element Number	Critical Buckling Load (N)	
	ANSYS	Present Study
15 x 15		55764
20 x 20		55724
25 x 25	55617 (15x15)	55662
30 x 30		55655

3.1. The effect of the stacking order

The effects of the stacking order on the first ten natural frequencies, critical buckling load, and the first unstable regions of the laminated composite arch plate frame structures are investigated. Five stacking orders, namely, C1, C2, C3, C4, and C5, are examined. The curvature of the structure is considered as $R_{xx}=2a$ and the aspect ratio is set as $a/b=1$. Table 3 gives the first ten natural frequency values of the laminated composite arch plate frame structure, having different stacking orders.

According to the results given in Table 3, the first ten natural frequencies are affected considerably by the stacking order. This is simply because of the difference in the stress components, Q_{ij} ($i,j=1,2,6$), of the material. Such a difference took place due to the change in stacking order. Another significant

outcome is the way the natural frequency values differ among the stacking orders.

Table 3. The first ten natural frequency values of the laminated composite arch plate frame structures having different stacking orders.

Natural Frequency (Hz)	C1	C2	C3	C4	C5
λ_1	6.880	4.114	6.558	6.640	6.589
λ_2	27.960	15.816	26.648	26.976	26.768
λ_3	34.545	23.735	33.512	34.168	33.882
λ_4	44.873	26.539	42.771	43.303	42.966
λ_5	45.060	31.209	43.410	44.047	43.705
λ_6	45.644	31.367	43.506	44.144	43.787
λ_7	49.210	37.784	47.285	48.028	47.645
λ_8	63.898	59.767	64.492	64.390	64.393
λ_9	64.798	67.517	65.289	65.225	65.208
λ_{10}	100.030	67.575	95.317	96.522	95.762

Figs. 7 and 8 show the laminated composite arch plate frame structure’s first unstable regions having different stacking orders. As seen in Figs. 7 and 8, the unstable region differs as the stacking order of the laminated composite frame structure changes. The distance of the first unstable regions to the origin can be ordered from the closest to farthest as C2, C3, C5, C4, and C1, respectively. This is because even though the stacking orders are different, the fundamental natural frequency values and the critical buckling load of the structures having C1, C3, C4, and C5 fiber angles do not change remarkably. The unstable region becomes narrow for the curved frame structure has C2 stacking order when compared with other stacking sequences. This is because the fiber angles of the first and the last layer effects both fundamental natural frequency and critical buckling load significantly. As the static load factor increases from 0 to 0.5, the first unstable regions move toward the origin and become narrow.

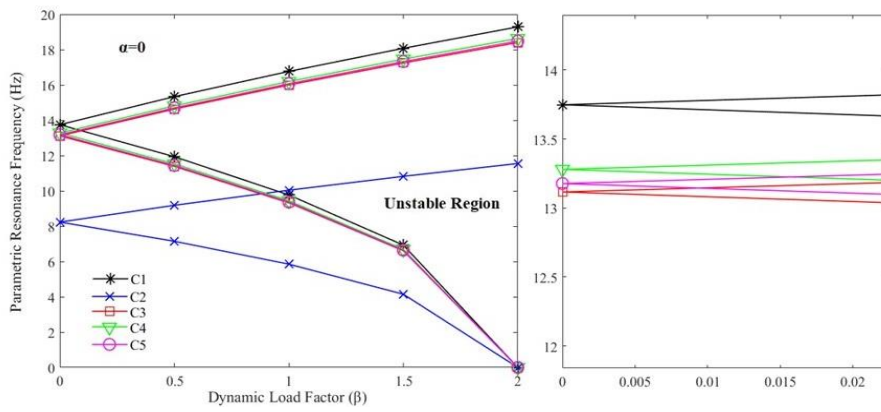


Figure 7. The first unstable regions ($\alpha = 0$) of the single-bay laminated composite curved plate frame structure having different stacking orders.

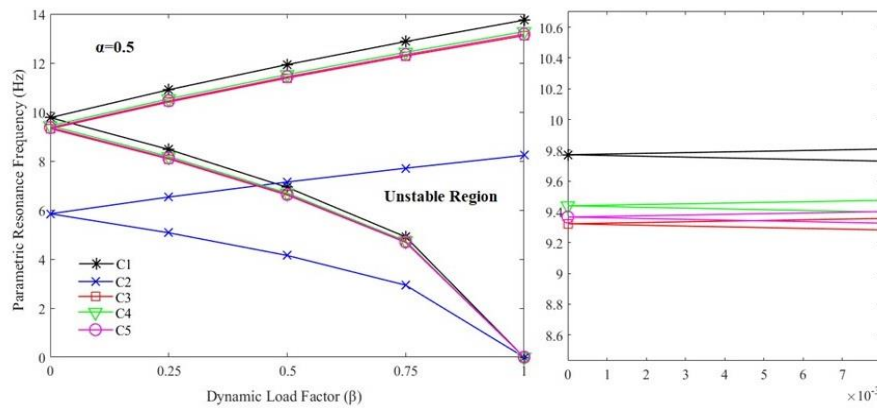


Figure 8. The first unstable regions ($\alpha = 0.5$) of the single-bay laminated composite curved plate frame structure having different stacking orders.

It is seen that as the structure’s stacking order is set as C2, the natural frequency values are considerably decreased when compared with other stacking orders. On the other hand, the natural frequencies C1, C3, C4, and C5 are close to each other. Such a situation reveals that the first and last layer’s fiber angles impact the natural frequency values. This is because of the highest bending moments, and consequently, bending stresses occur at that layers. Table 4 gives the critical buckling loads of the laminated composite arch plate frame structure having different stacking orders. According to the critical buckling load values given in Table 4, the stacking order affected the critical buckling load values just the way it affected the first ten natural frequency values of the laminated composite arch plate frame structures. The critical buckling load decreases slightly as the fiber angles of mid-layers increase. However, this decrement becomes significant when it comes to the first and last layers’ fiber angles.

Table 4. The critical buckling load values of the laminated composite arch plate frame structures having different stacking orders.

Stacking Order	Critical Buckling Load (N)
C1	55655
C2	19923
C3	50558
C4	51832
C5	51032

3.2. The effect of the radius of curvature

The effects of the radius of curvature on the first ten natural frequencies, critical buckling load, and the first unstable regions are investigated. For this purpose, four different radii of curvatures, $R_{xx}=1.5a$, $R_{xx}=2a$, $R_{xx}=2.5a$, and $R_{xx}=3a$ are considered. Table 5 gives the first ten natural frequency values of the single-bay C1 laminated composite arch plate frame structure with different curvatures. The aspect ratio of the structure is set as $a/b=1$.

Table 5. The first ten natural frequency values (Hz) of the C1 laminated composite curved plate frame structure.

Natural Frequency (Hz)	$R_{xx}=1.5a$	$R_{xx}=2a$	$R_{xx}=2.5a$	$R_{xx}=3a$
λ_1	6.823	6.880	6.905	6.908
λ_2	27.914	27.960	27.933	27.920
λ_3	34.575	34.545	34.450	34.387
λ_4	43.776	44.873	45.151	45.180
λ_5	44.741	45.060	45.177	45.195
λ_6	45.445	45.644	46.155	46.589
λ_7	48.161	49.210	50.051	50.563
λ_8	63.458	63.898	63.990	63.984
λ_9	64.964	64.798	64.705	64.622
λ_{10}	99.178	100.03	100.300	100.290

other as the radius of curvature increases from $1.5a$ to $2a$. Other modes remain the same when the radius of curvature changes. No matter which stacking order is considered, the radius of curvature has a negligible effect on the natural frequency values of the laminated composite curved plate frame structure.

Table 6 gives the critical buckling load values for four different radii of curvature of the single-bay curved plate frame structure.

Table 6. The critical buckling loads of the single-bay C1 laminated composite arch plate frames.

Radius of Curvature R_{xx}	P_{cr} (N)
$1.5a$	55974
$2a$	56315
$2.5a$	56483
$3a$	56580

According to the results given in Table 5, the change in the radius of curvature does not affect the first ten natural frequencies considerably. Even increasing the radius of curvature from $R_{xx}=1.5a$ to $R_{xx}=3a$, or decreasing in the opposite way changes the natural frequency value up to approximately 1.5 Hz. The mode shapes given in Appendix A indicate that the seventh and eighth modes shift to each

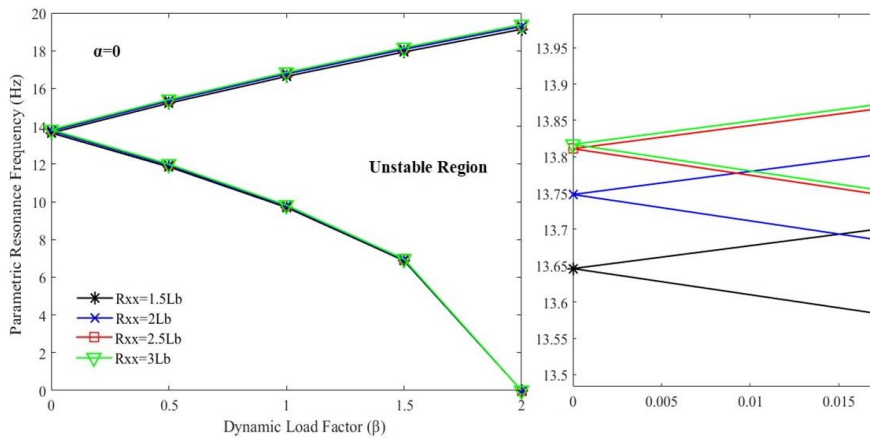


Figure 9. The first unstable regions of the single-bay laminated composite curved plate frame structure having C1 stacking order and different radius of curvatures for $\alpha = 0$

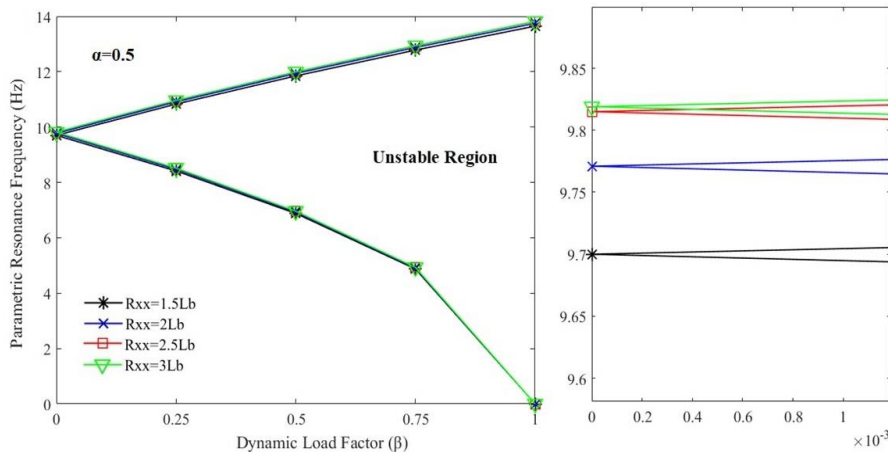


Figure 10. The first unstable regions of the single-bay laminated composite curved plate frame structure having C1 stacking order and different radius of curvatures for $\alpha = 0.5$

According to the critical buckling load values given in Table 6, as the radius of curvature of the single-bay laminated composite curved plate structure increases, the critical buckling load increases. However, such an increment can be accepted as negligible. Therefore, it can be interpreted that the change stiffness matrix of the structure in accordance with the radius of curvature is small. Figs. 9 and 10 show the first unstable regions of the single-bay C1 laminated composite arch plate frame structures with four different radii of curvatures considering two static load parameters $\alpha=0$ and $\alpha=0.5$.

It is seen from Figs. 9 and 10 that the radius of curvature affects the unstable region of the curved plate frame structure slightly. The unstable region moves toward the origin as the radius of curvature increases. On the other hand, the area of the unstable region does not change as the radius of curvature differs. The unstable region moves toward the origin and becomes narrow as the static load factor increases.

3.3. The effect of the aspect ratio

The effects of the aspect ratio on the first ten natural frequencies, critical buckling load, and the first unstable regions of the laminated composite arch plate frame structures are examined. Four different aspect ratios, $a/b=0.5$, $a/b=1$, $a/b=1.5$, and $a/b=2$ are taken into account. The radius of the curvature of the structures is set as $R_{xx}=2a$. Table 7 gives the change in the first ten natural frequency values and the critical buckling loads of the single-bay C1 laminated composite arch plate frame structure in accordance with the aspect ratio of the structure.

It is seen from Table 7 that the difference in aspect ratio affected certain modes considerably. As the aspect ratio increases from 0.5 to 2, the third - tenth natural frequencies increase more than 10Hz. For the eighth - tenth modes, such an increment differs between 50 - 70 Hz. The first and second natural frequencies do not change significantly as the aspect ratio varies. While these interpretations are valid for C3, C4, and C5 stacking orders, the structure with C2 fiber orientation behaves differently than those of other stacking orders.

Table 7. The first ten natural frequency values of the single-bay C1 laminated composite arch plate frames having four different aspect ratios

Natural Frequency (Hz)	a/b=0.5	a/b=1	a/b=1.5	a/b=2
λ_1	6.885	6.880	6.869	6.870
λ_2	27.990	27.960	28.296	27.904
λ_3	29.762	34.545	41.282	44.808
λ_4	41.278	44.873	45.396	45.580
λ_5	44.891	45.060	46.182	48.814
λ_6	45.642	45.644	51.140	57.295
λ_7	45.953	49.210	54.349	59.541
λ_8	46.311	63.898	94.229	99.876
λ_9	47.179	64.798	95.065	120.750
λ_{10}	54.567	100.030	104.190	125.470

Most of the natural frequencies and corresponding mode shapes of the C2 stacking order are obtained dissimilar to those of C1, C3, C4, and C5, as seen in Table 8 and Appendix B.

Table 8. The first ten natural frequency values of the single-bay C2 laminated composite arch plate frames having four different aspect ratios

Natural Frequency (Hz)	a/b=0.5	a/b=1	a/b=1.5	a/b=2
λ_1	4.120	4.116	4.112	4.108
λ_2	16.749	16.725	16.705	16.688
λ_3	19.626	26.390	26.824	26.807
λ_4	26.115	26.846	27.286	27.268
λ_5	26.875	27.308	34.689	43.435
λ_6	27.337	31.613	38.858	46.892
λ_7	28.809	33.378	39.873	47.613
λ_8	34.302	59.861	59.798	59.739
λ_9	34.922	66.908	72.276	72.215
λ_{10}	51.313	67.379	81.927	82.100

According to results given in Table 3.8, the third and fifth - tenth natural frequencies are affected by the aspect ratio, considerably. Among these modes, the eighth-tenth modes increases between 25-40 Hz as the aspect ratio changes from 0.5 to 2. Comparing the results obtained for C2 and other stacking sequences, it is interpreted that the natural frequencies of C2 are affected less than those of C1, C3, C4, and C5. Table 9 gives the critical buckling load of the single-bay C1 laminated composite arch plate frames with various aspect ratios.

Table 9. The critical buckling loads of the single-bay C1 laminated composite arch plate frames having four different aspect ratios

Aspect Ratio (a/b)	P_{cr} (N)
0.5	111510
1	55655
1.5	37033
2	27720

It is seen from Table 9 that the critical buckling load decreases as the aspect ratio increases. The same behavior is observed for all stacking orders.

Figs. 11 and 12 show the first unstable regions of such structure as the aspect ratio changes.

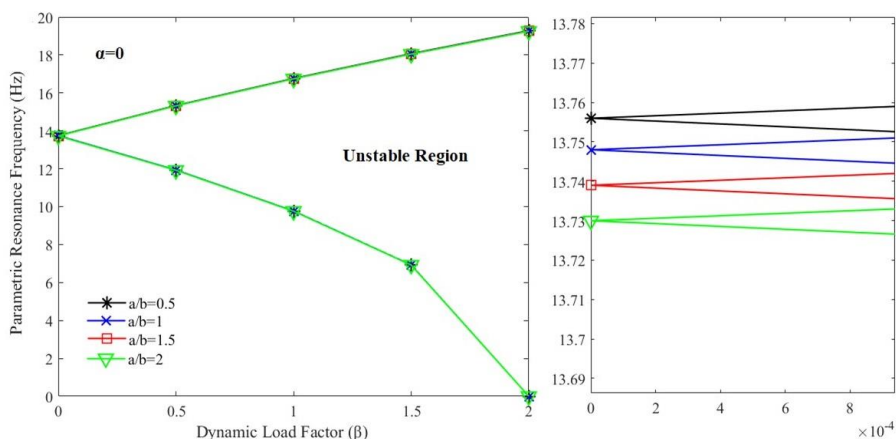


Figure 11. The first unstable regions ($\alpha = 0$) of the single-bay laminated composite curved plate frame structure having C1 stacking order and different aspect of ratios

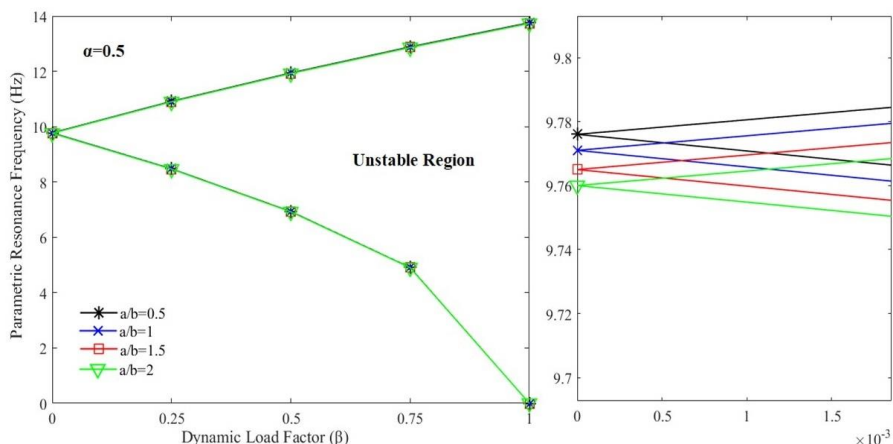


Figure 12. The first unstable regions ($\alpha = 0.5$) of the single-bay laminated composite curved plate frame structure having C1 stacking order and different aspect of ratios

It is inferred from Figs. 11 and 12 that the aspect ratio of the curved frame structure does not affect the instability region considerably. The unstable region moves towards the origin as the aspect ratio increases. As the dynamic load factor increase, the unstable region slightly widens and moves away from the origin.

3.4. Two-bay structure

The first ten natural frequencies, critical buckling loads, and the first unstable regions of the laminated composite two-bay curved plate frame structure shown in Fig.13(a) are evaluated. The loading case shown in Fig.13(b) is the same as that of the single-bay structure. The radius of curvature is chosen as $R_{xx}=2a$ and the aspect ratio is considered as $a/b=1$. All analyses are performed under fixed from all ends of columns.

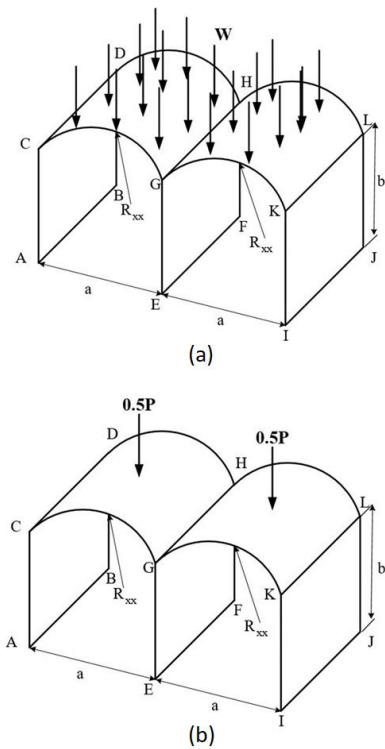


Figure 13. (a)The distributed loading condition and (b) the equivalent point loading condition of two-bay laminated composite curved plate frame structure

According to the results given in Table 10, the first seven natural frequencies of the two-bay structure are higher than those of the single-bay structure. Contrarily, the eighth - tenth natural frequencies of the two-bay structure are lower than those of single - bay structure. Similar interpretations made for the two-bay curved plate frame structure with C1 stacking order can be made for other stacking orders. Comparing the mode shapes of the two-bay

structure and single-bay structure with C1 stacking order given in Appendices A and C, it is seen that the first, second, and fifth modes of the single-bay and two-bay structure are identical whereas other modes are different. Among those different modes, the sixth and eighth modes of the two-bay structure are completely different from those of the single-bay structure while the rest are shifted modes (i.e., the third mode of the single-bay structure shifted to the fourth mode for the two-bay structure). The critical buckling load of the two-bay structure is higher than that of the single-bay structure, as expected.

Table 10. The first ten natural frequencies and critical buckling load of the laminated composite two-bay curved plate frame structure

Natural Frequency (Hz)	Two-Bay Structure	Single-Bay Structure
λ_1	7.237	6.880
λ_2	30.478	27.960
λ_3	39.935	34.545
λ_4	45.817	44.873
λ_5	49.265	45.060
λ_6	51.555	45.644
λ_7	52.266	49.210
λ_8	57.355	63.898
λ_9	58.161	64.798
λ_{10}	61.612	100.030
Critical Buckling Load (N)	87091	56315

Figs. 14 and 15 show the first unstable regions of the laminated composite two-bay and single-bay curved plate frame structure with C1 stacking order

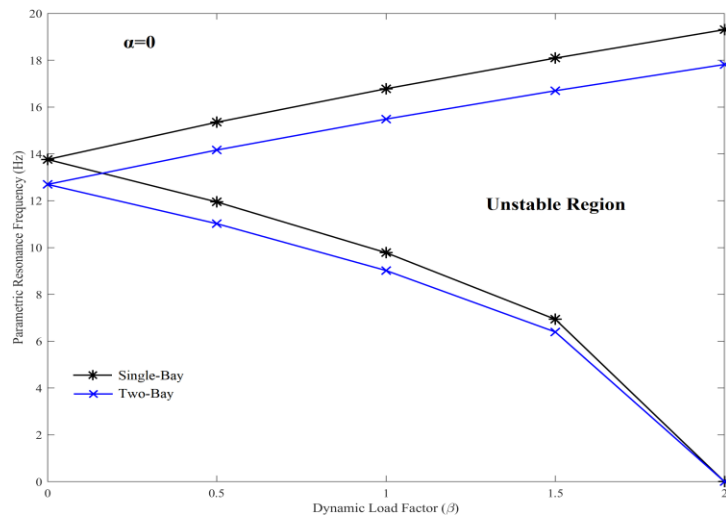


Figure 14. The first unstable regions ($\alpha = 0$) of the two-bay and single-bay laminated composite curved plate frame structure having C1 stacking order.

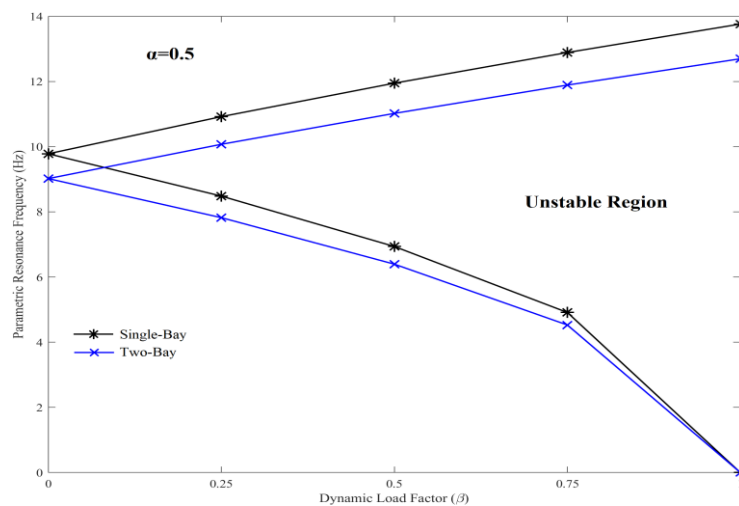


Figure 15. The first unstable regions ($\alpha = 0.5$) of the two-bay and single-bay laminated composite curved plate frame structure having C1 stacking order.

According to Figs. 14 and 15, the first unstable regions of the two-bay structure are closer than those of the single-bay structure. The area of the first unstable regions of the single-bay and two-bay structures are almost the same. The first unstable regions move toward the origin as the static load factor increases from 0 to 0.5 for both single-bay and two-bay structures.

4. Conclusions

In this paper, dynamic and buckling analysis of the laminated composite arch plate frame structures is investigated. The first ten natural frequencies, critical buckling loads, and the first unstable regions are examined considering the radius of curvature, aspect ratio, and fiber orientation of these structures. Besides, the two-bay structure is investigated. The following conclusions are drawn.

- Stacking orders have a considerable effect on the natural frequencies, critical buckling load, and the first unstable regions. It is seen that the fiber angles of the first and last layers have the most impact on the dynamic characteristics of the structure. On the other hand, the fiber angles of the mid-layers also affect the dynamical properties of the curved plate frame structure. However, such an impact is small when compared with that of the fiber angles of the first and last layers.
- The radius of curvature of the laminated composite arch plate frame structures has a negligible impact on the first ten natural frequency

values, the critical buckling load, and the first unstable regions.

- As the aspect ratio increases, all the natural frequency values increase, except the first and the second frequencies. Similarly, the critical buckling load values increase in accordance with the increment of the aspect ratio. On the other hand, the unstable region does not change significantly. Without changing the width, the unstable region moves slightly toward the origin as the aspect ratio increases.
- The first seven natural frequencies of the two-bay structure are higher than those of the single-bay structure, whereas it is the opposite for the eighth - tenth natural frequencies. The critical buckling load of the two-bay structure is higher than that of the single-bay structure, as expected. The first unstable regions of the two-bay structure are closer to the origin when compared with those of the single-bay structure. The area of the first unstable regions of these structures is the same. The increment of the static load factor moves the unstable region toward the origin for both structures.
- The difference in the radius of curvature of the laminated plate frame structure does not change the mode shapes of the structure. Contrarily, the aspect ratio and the stacking order affect the mode shapes considerably. The first two modes are the same for every stacking order, the radius of curvature, and stacking ratio. On the other hand, other modes differ with respect to both

stacking order and aspect ratio of the curved plate frame structure. It is seen from Appendix B that the mode shapes of the curved plate frame structure having C1, C3, C4, and C5 stacking order are the same, except for the third and fourth modes. On the other hand, the mode shapes of the structure having C2 is different for several modes. Such a difference becomes more apparent as the aspect ratio of the structure changes.

- It is seen that the first, second and fifth modes of the single-bay and two-bay curved plate frame structures are identical. On the other hand, the sixth and eighth modes of the two-bay structure are completely different from those of the single-bay structure while the rest are shifted modes (i.e., the third mode of the single-bay structure shifted to the fourth mode for the two-bay structure).

Acknowledgement

The Authors gratefully acknowledge the Central Research Facility at the Abdullah Gul University for the availability and use of X-ray diffractometer (XRD). This work is also supported by the Scientific and Technological Research Council of Turkey through the program of Starting Research and Development Projects (TUBITAK 3001-118M253).

5. References

Abualnour, M., Houari, M.S., Tounsi, A., Bedia, E.A., and Mahmoud, S.R., 2018. A novel quasi-3d trigonometric plate theory for free vibration analysis of advanced composite plates. *Composite Structures*, **184**, 688–697.

Bolotin, V.V., 1964. *The dynamic stability of Elastic Systems*, Holden-Day.

Bourada, F., Amara, K., and Tounsi, A., 2016. Buckling analysis of isotropic and orthotropic plates using a novel four variable refined plate theory. *Steel and Composite Structures*, **21**(6), 1287–1306.

Chen, J.E., Zhang, W., Sun, M., Yao, M.H., and Liu, J., 2017. Free vibration analysis of composite sandwich plates with different truss cores. *Mechanics of Advanced Materials and Structures*, **25**(9), 701–713.

Chikh, A., Tounsi, A., Hebali, H., and Mahmoud, S.R., 2017. Thermal buckling analysis of cross-ply

laminated plates using a simplified HSDT. *Smart Structures and Systems*, **19**(3), 289–297.

Demir, Ç., Ersoy, H., Mercan, K., and Civalek, Ö., 2017. Free vibration analysis of annular sector plates via conical shell equations. *Curved and Layered Structures*, **4**(1), 146–157.

Dey, P. and Singha, M. K., 2006. Dynamic stability analysis of composite skew plates subjected to periodic in-plane load. *Thin-Walled Structures*, **44**(9), 937–942.

Fang, J., Zheng, S., Xiao, J., and Zhang, X., 2020. Vibration and thermal buckling analysis of rotating nonlocal functionally graded nanobeams in thermal environment. *Aerospace Science and Technology*, **106**, 106146.

Fazilati, J., 2017. Stability analysis of variable stiffness composite laminated plates with delamination using spline-FSM. *Latin American Journal of Solids and Structures*, **14**(3), 528–543.

Hao, P., Yuan, X., Liu, H., Wang, B., Liu, C., Yang, D., and Zhan, S., 2017. Isogeometric buckling analysis of composite variable-stiffness panels. *Composite Structures*, **165**, 192–208.

Marjanović, M., Kolarevic, N., Nefovska-Danilovic, M., and Petronijevic, M., 2017. Shear deformable dynamic stiffness elements for a free vibration analysis of composite plate assemblies – part II: Numerical examples. *Composite Structures*, **159**, 183–196.

Petyt, M., 2015. *Introduction to finite element vibration analysis*, Cambridge University Press.

Rezaiee-Pajand, M., Sobhani, E., and Masoodi, A.R., 2020. Free vibration analysis of functionally graded hybrid matrix/fiber nanocomposite conical shells using multiscale method. *Aerospace Science and Technology*, **105**, 105998.

Samukham, S., Raju, G., Wu, Z., and Vyasrayani, C.P., 2018. Dynamic instability analysis of variable angle tow composite plate with delamination around a cut-out. *Mechanics of Advanced Materials and Structures*, **26**(1), 62–70.

Serdoun, S.M.N. and Hamza Cherif, S.M., 2016. Free vibration analysis of composite and sandwich plates

by alternative hierarchical finite element method based on Reddy's C1 HSDT. *Journal of Sandwich Structures & Materials*, **18**(4), 501–528.

Shafei, E., Faroughi, S., and Rabczuk, T., 2019. Isogeometric HSDT approach for dynamic stability analysis of general anisotropic composite plates. *Composite Structures*, **220**, 926–939.

Shankar, G. and Mahato, P.K., 2017. Vibration analysis and control of delaminated and/or damaged composite plate structures using finite element analysis. *Materials at High Temperatures*, **34**(5-6), 342–349.

Thakur, B.R., Verma, S., Singh, B.N., and Maiti, D.K., 2020. Dynamic analysis of folded laminated composite plate using nonpolynomial shear deformation theory. *Aerospace Science and Technology*, **106**, 106083.

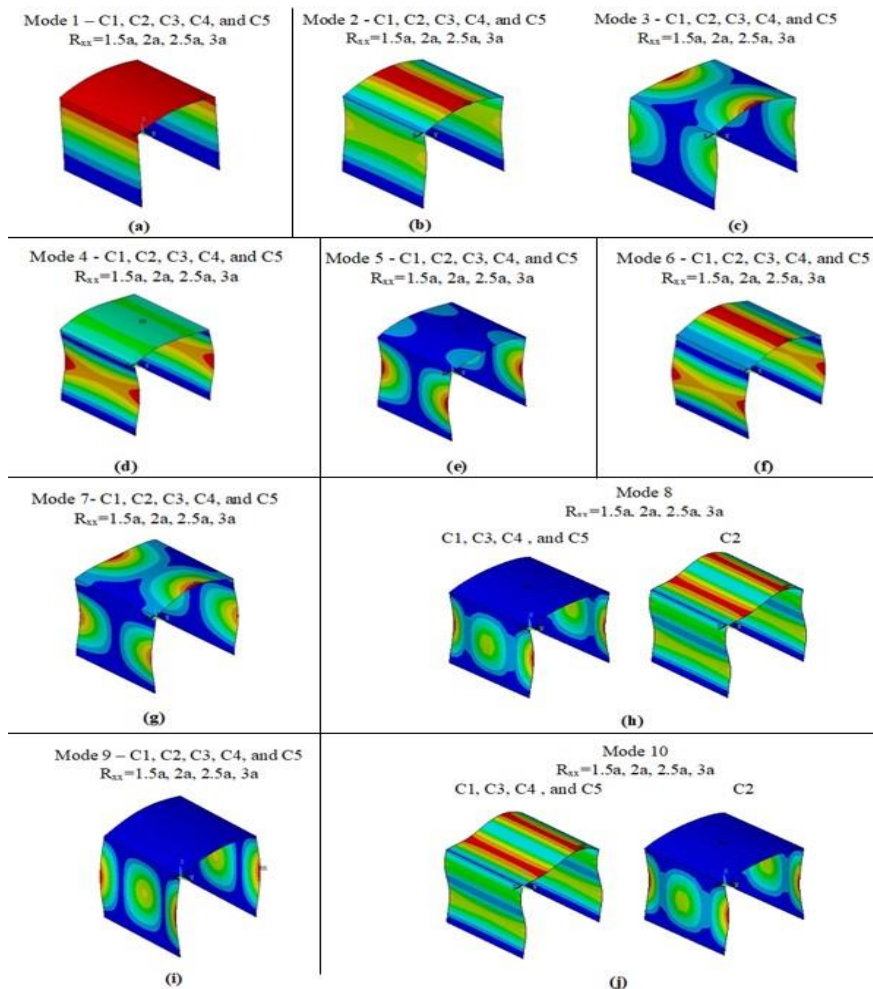
Tornabene, F., Fantuzzi, N., and Baccocchi, M., 2018. Strong and weak formulations based on differential and integral quadrature methods for the free vibration analysis of composite plates and shells: Convergence and accuracy. *Engineering Analysis with Boundary Elements*, **92**, 3–37.

Vidal, P., Gallimard, L., and Polit, O., 2019. Free vibration analysis of composite plates based on a variable separation method. *Composite Structures*, **230**, 111493.

Zghal, S., Frikha, A., and Dammak, F. (2018). Mechanical buckling analysis of functionally graded power-based and carbon nanotubes-reinforced composite plates and curved panels. *Composites Part B: Engineering*, **150**, 165–183.

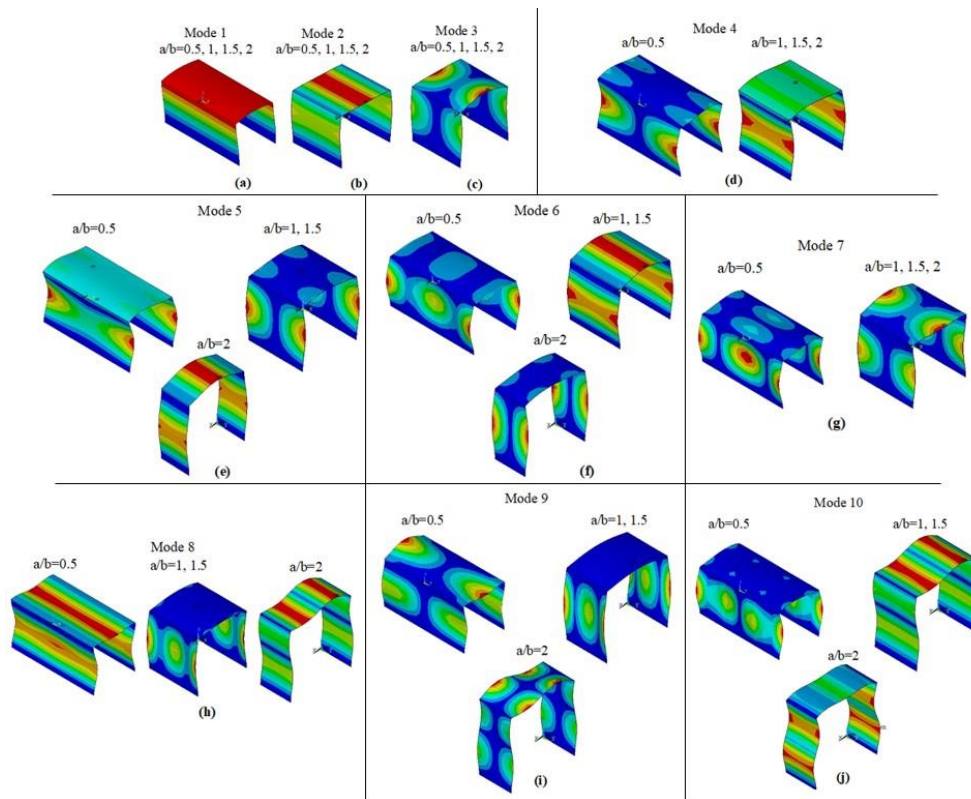
Appendix

Appendix – A: The First Ten Mode Shapes of the Single-Bay Curved Plate Frame Structure Having Different Stacking Orders

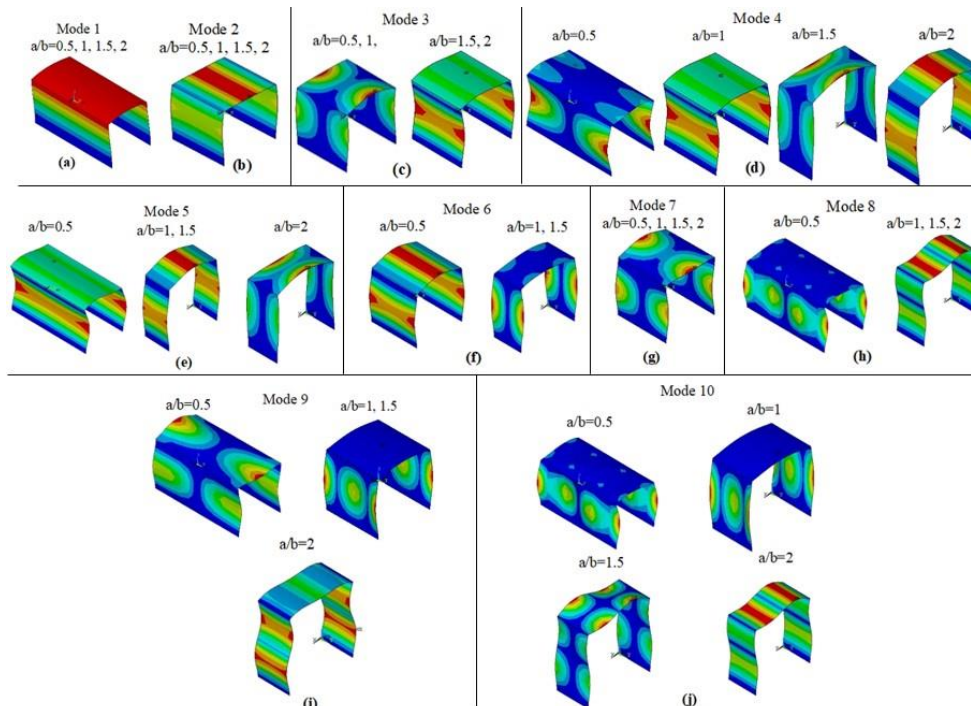


Appendix – B: The First Ten Mode Shapes of the Single-Bay Curved Plate Frame Structure Having Different Aspect Ratios for C1, C2, C3, C4, and C5 Stacking Orders

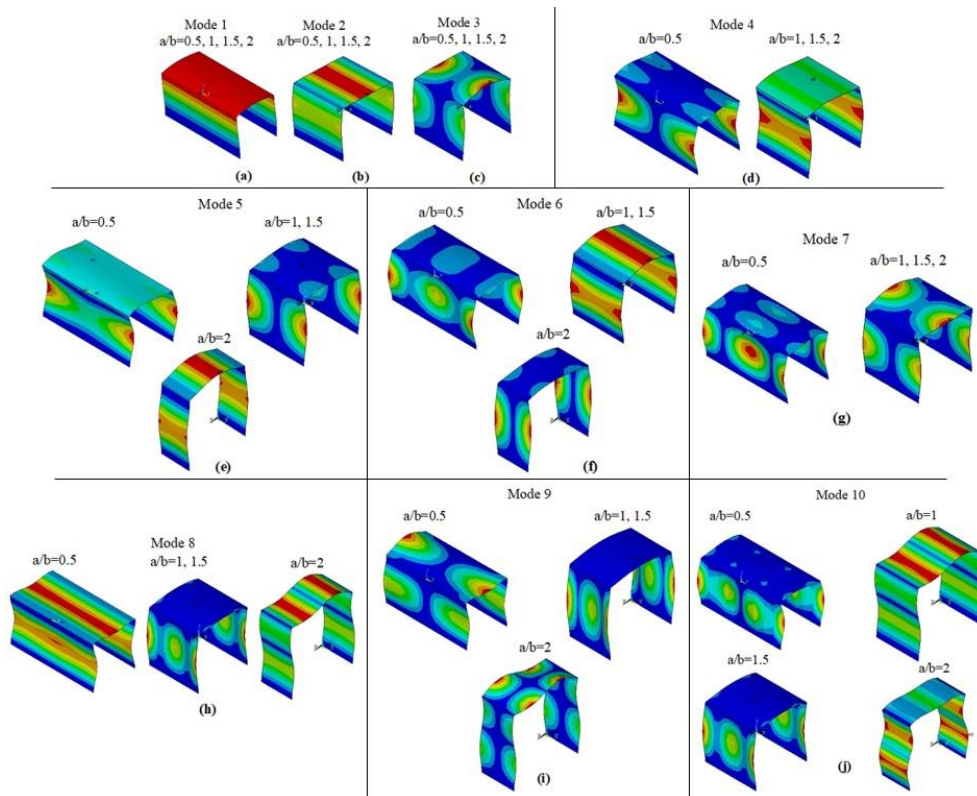
C1



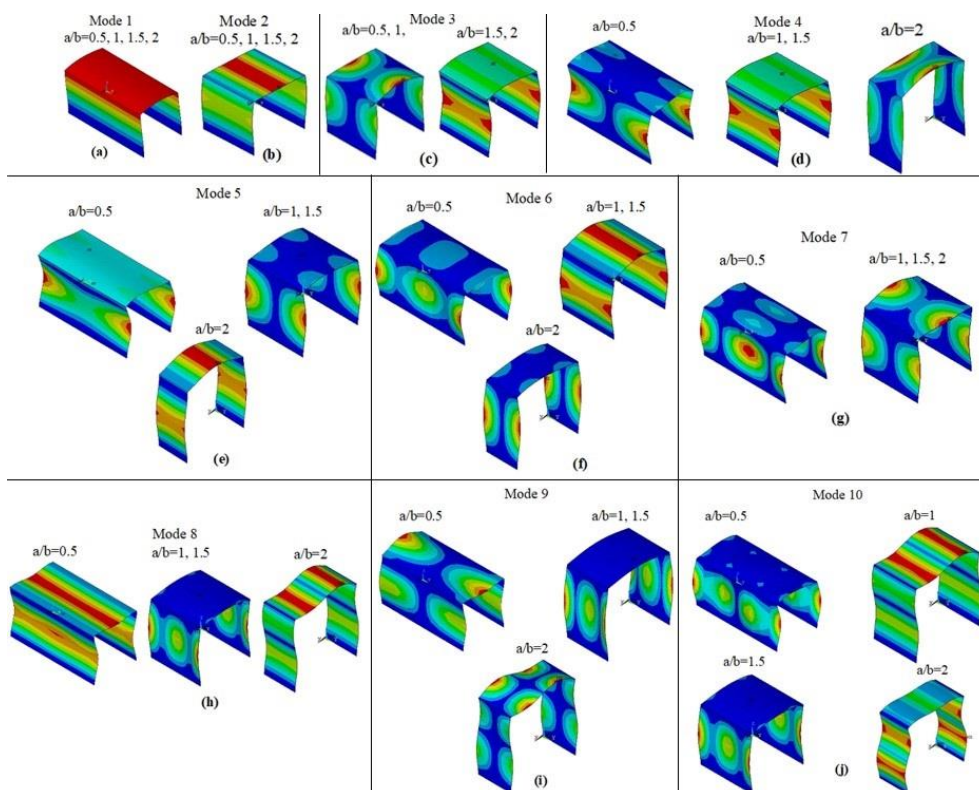
C2



C3



C4 & C5



Appendix – C: The First Ten Mode Shapes of the Two-Bay Curved Plate Frame Structure Having C1 Stacking Order and $a/b=1$ Aspect Ratio

